SENSORS IN THE DEEP SEA

Tiny variations in temperature, pressure and currents can be measured with modern electronics. Problems arise, though, when variations in one parameter affect the reading of another. Work on the Deep-Sea Capsule has found some solutions.

DOUGLAS R. CALDWELL, FRANK E. SNODGRASS and MARK H. WIMBUSH

Great advances in deep-sea research have become possible with recent improvements in electronic instrumentation and development of large computers. Many of today's instrumental techniques in oceanography have resulted from developments associated with space exploration. Indeed similarities exist between outer-space and ocean-depth studies. Manned space vehicles have counterparts in deep submersible submarines with life-support systems that carry men to observe in the greatest depths of the sea, and instrumented satellites and space probes have counterparts in a new family of unmanned capsules that carry electronic systems with delicate sensors to measure and record the deep-sea environment. Electronic recording systems for instrumented capsules must be light and compact and have low power consumption and high reliability.

In oceanography, component needs for digital logic systems are usually met by available techniques and commercial equipment easily adapted to capsules. Problems such as intermittent gaps in the data, aliasing and least-count noise (caused by quantizations of the signal in time and magnitude respectively), and modulo effects (which occur when the most significant bits of the data are discarded

for recording economy) are well understood.¹ In a carefully engineered recording system, these problems present no fundamental difficulties to the experimenter. Digital systems functioning properly perform in an explicit way that can be described precisely when the data are analysed.

Sensor problems

The sensor and its associated electronics present a problem quite different from those of the digital recording system. The device does not function in an explicit way that allows precise interpretation of the data; the sensor may be functioning properly yet produce data that are not solely dependent on the parameter to be measured. Operation of the sensor must be understood in detail. Then readings can be interpreted in a reasonable manner and realistic limits of operation can be applied so that the unit will not be used under unsuitable conditions.

Understanding of the sensor is accomplished by calibrating and testing, but tests in the laboratory may not represent conditions under which measurements are to be made. This is particularly true of deep-sea sensors. Resolution and dynamic range of measurements have been increased until sensor self-noise is the limiting

factor. The laboratory environment, however, is so unstable, compared to that of the sea floor and the noise level of the sensors, that direct measurement of instrumental noise is impossible. Moreover sensors must be calibrated over comparatively large ranges, but on the sea floor they operate within very narrow limits. Temperature sensors are calibrated over a 10°C range whereas sea-floor temperature signals vary by only a few millidegrees; pressure sensors are calibrated over the range of 5500 meters of water pressure whereas sea-floor pressure signals vary only by 1 meter. Overall calibration may not be correct for use in the sea. Final evaluation of the sensor cannot be made except under actual operating conditions.

With specially designed pressure, temperature and current sensors and recording capsule, we are able to measure the deep-sea tide. Many people have speculated on the midocean tide during the last hundred years, but cotidal charts of the ocean, showing predicted phase contours for a given tide constituent, differ greatly according to the assumptions made.

Until recently, measurements of the tide had been made only in coastal waters. By measuring pressure and current fluctuations in the deep sea, we are determining the properties of

the tide away from the ocean boundaries. We have also used the same apparatus to investigate the thermal and dynamic properties of the seabottom boundary layer.

Deep-sea capsule

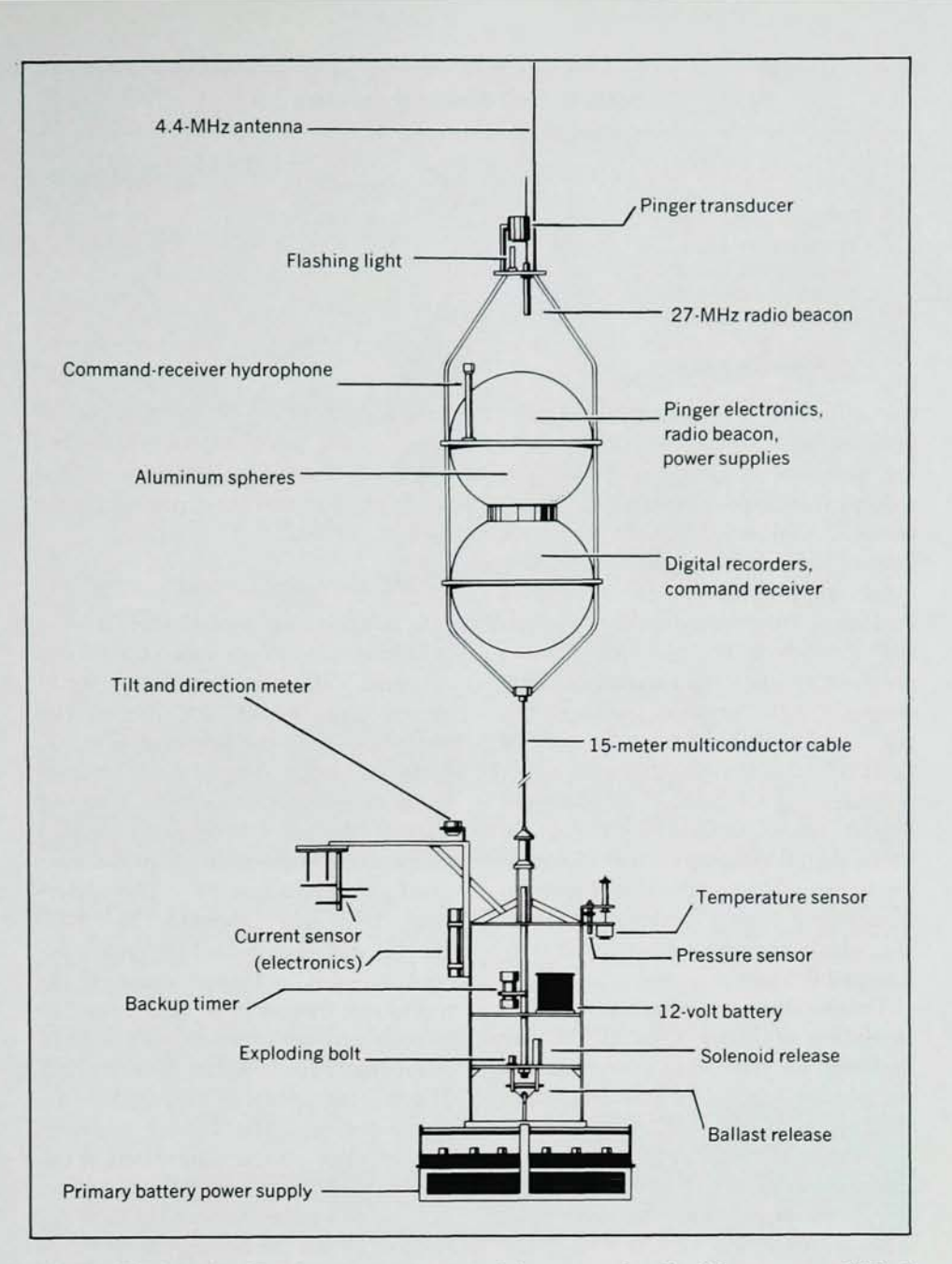
Our deep-sea instrument capsule² (figure 1) is assembled in two parts: the buoyant 56-cm aluminum spheres (figure 2), which house digital data recorders, the acoustical system, radio beacons, flashing lights, etc. and the instrument frame (figure 3), which supports various sensors, release mechanisms, the tilt and direction meter, and a battery for the radio beacon. The spheres and instrument frame are connected by a 15-meter cable. A ballast of automobile batteries holds the equipment firmly on the bottom while supplying power to the system. Because of their buoyancy the spheres are tethered at the upward end of the electrical cable where they cause no interference with measurements made near the bottom.

The capsules are dropped from a surface ship to the sea floor where they remain for periods ranging from several days to several weeks. The ship can return to port while data are accumulated by computer-compatible magnetic tape recorders in the capsules. When the ship returns, the instrument capsules are recalled to the surface by acoustical commands transmitted from the ship. On command the capsule disconnects from the ballast with a solenoid release or an exploding bolt, then ascends to the surface by its own buoyancy. On the surface, radio beacons and a flashing light provide homing signals for the final recovery.

Adaptable to a variety of experiments, the capsule is presently studying deep-sea tides by recording fluctuating pressure and water velocity on the deep-sea floor. We have made about 40 drops to 4-km depths. Some of these installations were expressly intended to evaluate sensors, and others were designed to study tides and the ocean-bottom boundary layer.

Pressure measurements

Tide measurements are made by sensing water pressure with the Vibrotron pressure sensor manufactured by the United Control Corp. A tungsten filament about 1-cm long is stretched in a magnetic field and encased in a dry atmosphere at low pressure. One end is attached to a rigid frame and



DEEP-SEA CAPSULE. Sensors are separated from recorders by 15 meters. -FIG. 1



INTO THE SEA. Technicians prepare to drop capsule into the ocean.

Table 1. Sea-Bottom Parameters

	Mean value	Daily variation range
Pressure (dynes/cm²)	4×10^{8}	105
Temperature (°C)	2	0.001
Water speed (cm/sec)	3	6
Boundary-layer thickness (meters)	5	10
Direction of flow (deg)		360

the other to a diaphragm. Under pressure the diaphragm inflects causing the wire tension, and hence the natural frequency of vibration, to decrease. Connected in the feedback loop of an amplifier, the wire makes a variable-frequency oscillator with a frequency f that is a function of pressure $P: f^2 = \alpha P + \gamma$. A Vibrotron pressure gauge with a range of 5500 meters of water pressure (8000 pounds per square inch) has a sensitivity $\alpha/2f$ of -2.0 Hz per meter of water pressure at typical ocean-bottom depths (4000 meters). By conventional digital techniques the Vibrotron frequency when sampled for 2 minutes is measured to an accuracy of 6×10^{-4} Hz, which provides a least-count resolution of 0.5 mm.

Temperature measurements with a resolution of better than 10⁻³°C are required for Vibrotron corrections to the nearest 1 mm of equivalent water pressure. Using the quartz-crystal oceanographic-temperature probe manufactured by Hewlett Packard Corp, we readily get measurements with a resolution of 10⁻⁵°C. The

temperature probe provides a correction for the pressure transducer but also data of great interest in a general study of conditions that prevail on the floor of the sea.

Temperature and current

The temperature probe consists of a cylindrical pressure case containing two solid-state crystal oscillators, mixer circuit and output amplifier. crystals, one LC-cut (circular, C mode, $\phi = 11.116 \deg, \theta = 13 \deg$ for high linear temperature sensitivity, and one AT-cut ($\phi = 0$, $\theta = 35 \text{ deg}$) for zero temperature coefficient, make the temperature measurements. The difference frequency changes by 1000 Hz/°C, and zero output frequency occurs at -5° C. Measurement of the transducer frequency in cycles per 120 seconds produces records with a leastcount resolution of better than 10-5°C. The AT-cut crystal is mounted in the pressure case. The LC-cut temperature-sensitive crystal is mounted at the end of a 2.5-mm-diameter stainlesssteel tube to isolate it from the heat developed by the electronics.





Douglas R. Caldwell, assistant professor of oceanography at Oregon State University, specializes in geophysical fluid mechanics. He received his PhD in physics from the University of Chicago in 1963, spent a year at Cambridge University and then worked at the Institute of Geophysics and Planetary Physics in La Jolla until 1968.

Frank E. Snodgrass remained with the University of California after receiving his master's degree in electrical engineering to work in oceanography, first with the Institute of Engineering Research at Berkeley, then at the Scripps Institution of Oceanography and presently at the Institute of Geophysics and Planetary Physics.

Mark Wimbush, born in Kenya, received his BA in physics from Oxford, a master's in mathematics from the University of Hawaii and a PhD in oceanography at the University of California, San Diego. He is now doing postdoctoral work in deep-sea physical oceanography at the Institute of Geophysics and Planetary Physics in La Jolla.

We have measured ocean-bottom currents with a specially designed probe containing an indirectly heated thermistor (figure 3) whose temperature depends on the cooling flow of the water.3 A threshold below that normally achieved by mechanical devices low power consumption, high reliability and a frequency output compatible with the recording system were major design considerations. Flow magnitude is measured by a matched pair of probes mounted vertically with one probe heated and one not. Ambient temperature effects are canceled, and temperature difference is a measure of Maximal cooling of the current. heated element occurs when water flow is in a plane perpendicular to the longitudinal axis of the element. Cooling is independent of direction in that plane. The flow is assumed to be nearly horizontal near the sea floor.

A pair of heated probes mounted horizontally at right angles provide good directional sensitivity. For a given temperature difference, however, four directions are possible. The ambiguity is resolved by correlating the angles measured by two pairs of probes displaced 135 deg and by taking advantage of the asymmetry introduced in the directional response by the mounting post (which disturbs in different ways the upstream and downstream parts of the flow). Directional calibrations are sensitive to flow speed as well. Given measurements from three pairs of probes, the computer interpolates calibration data to determine flow direction and magnitude.

Sea-bottom environment

Any equipment placed in the deep ocean must be designed to withstand high pressure and sea-water corrosion. Of special importance in selecting or designing transducers is the "quietness" of the environment: Temperature is exceedingly steady, current feeble, relative pressure fluctuations very small.

Some sea-bottom parameters are shown in table 1. The daily variations shown are principally due to tides. Figure 4 shows three days of current, pressure and temperature data.

The hydrodynamic boundary layer is about 5 meters thick, but one third of the velocity change occurs in the first few centimeters above bottom. The next meter has the logarithmic profile typical of a turbulent boundary layer. In the upper part of the

layer the speed rises slowly to its value in the free stream. The flow being tidal, its speed and direction are constantly changing. Because geothermal heat from the earth's interior flows up through the ocean floor, there is also a thermal boundary layer with the same vertical scales. Mark H. Wimbush and Walter H. Munk⁴ consider these boundary layers in detail. The pressure transducer senses a weighted average of the water height, the principal contribution coming from a vertical 120-deg cone with apex at the transducer.

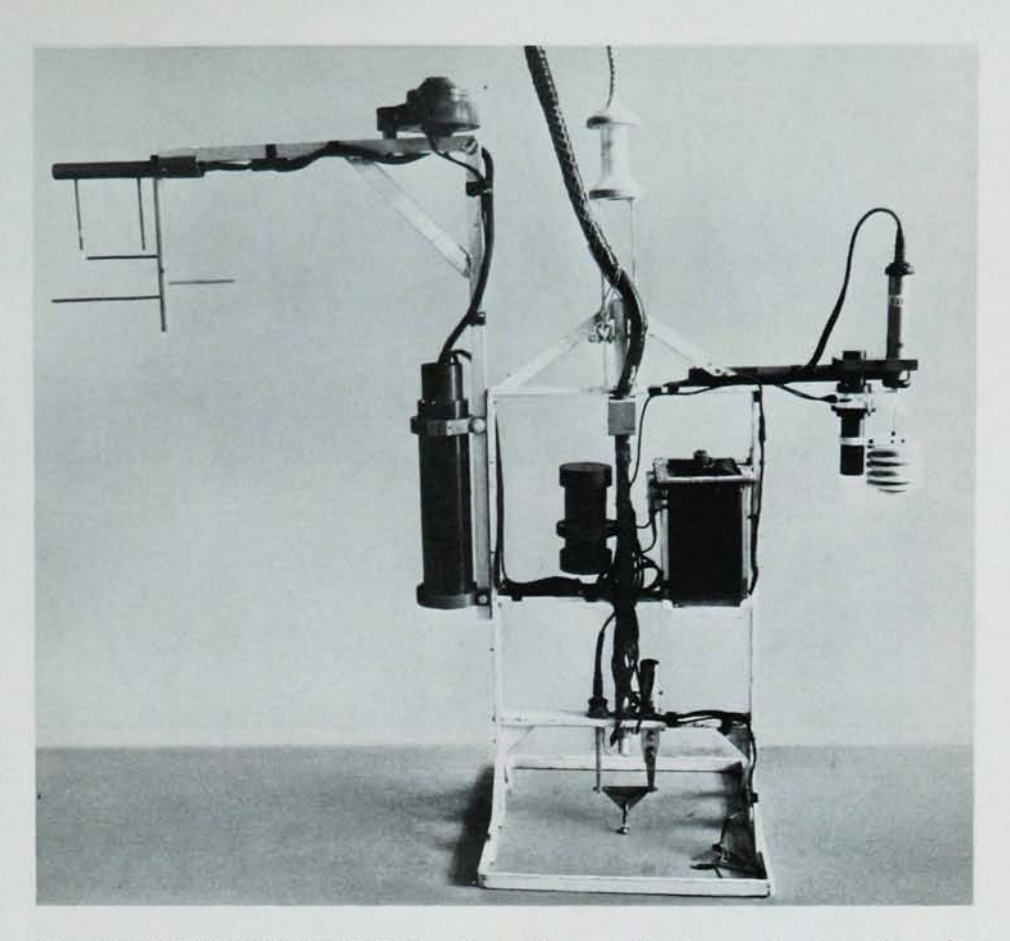
Pressure-sensor calibration

With the Vibrotron pressure sensor in a temperature-controlled water bath. pressure is applied in increments of 1000 psi from 0 to 8000 psi (+ atmospheric pressure) by means of a dead-weight tester. The sensor output is assumed to be smooth and continuous between these large pressure increments. A polynomial calibration curve is fitted to the data (f^2 vs P) by the least-squares method. The frequency deviates slightly from the expected square law. By repeating the pressure calibration at several temperatures between 0° and 20°C, and then cross plotting the data, a temperature calibration at each pressure increment is obtained.

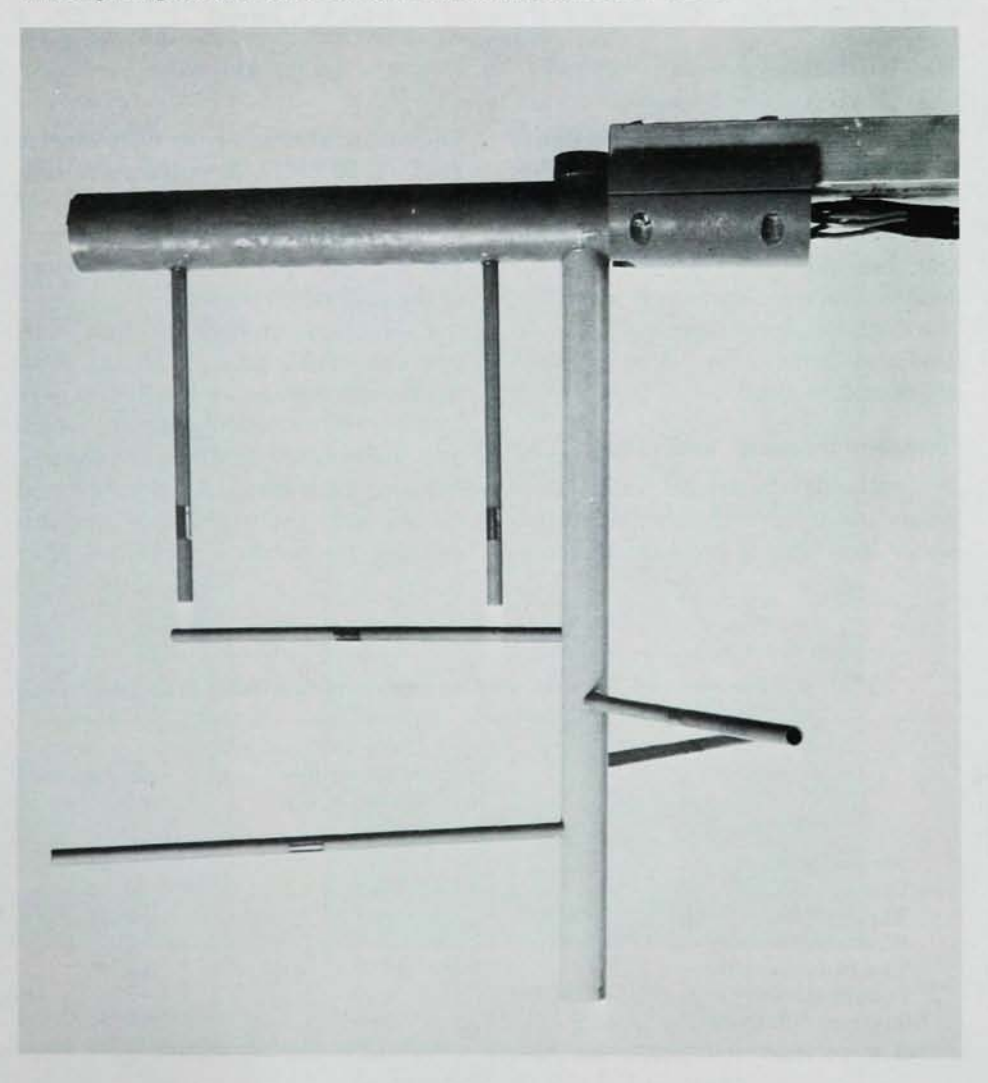
When calculating the absolute pressure from measurements made while the capsule is falling, full account is taken of the pressure and temperature calibration. When calculating the pressure fluctuations after the capsule has stabilized on bottom, only the slopes of the calibration curves are used. Interpolation of the calibration data provides both pressure and temperature sensitivities at the mean pressure and temperature of the deep-sea experiment. The sensor can be assumed to respond linearly at the calculated sensitivities over the range of bottom fluctuations.

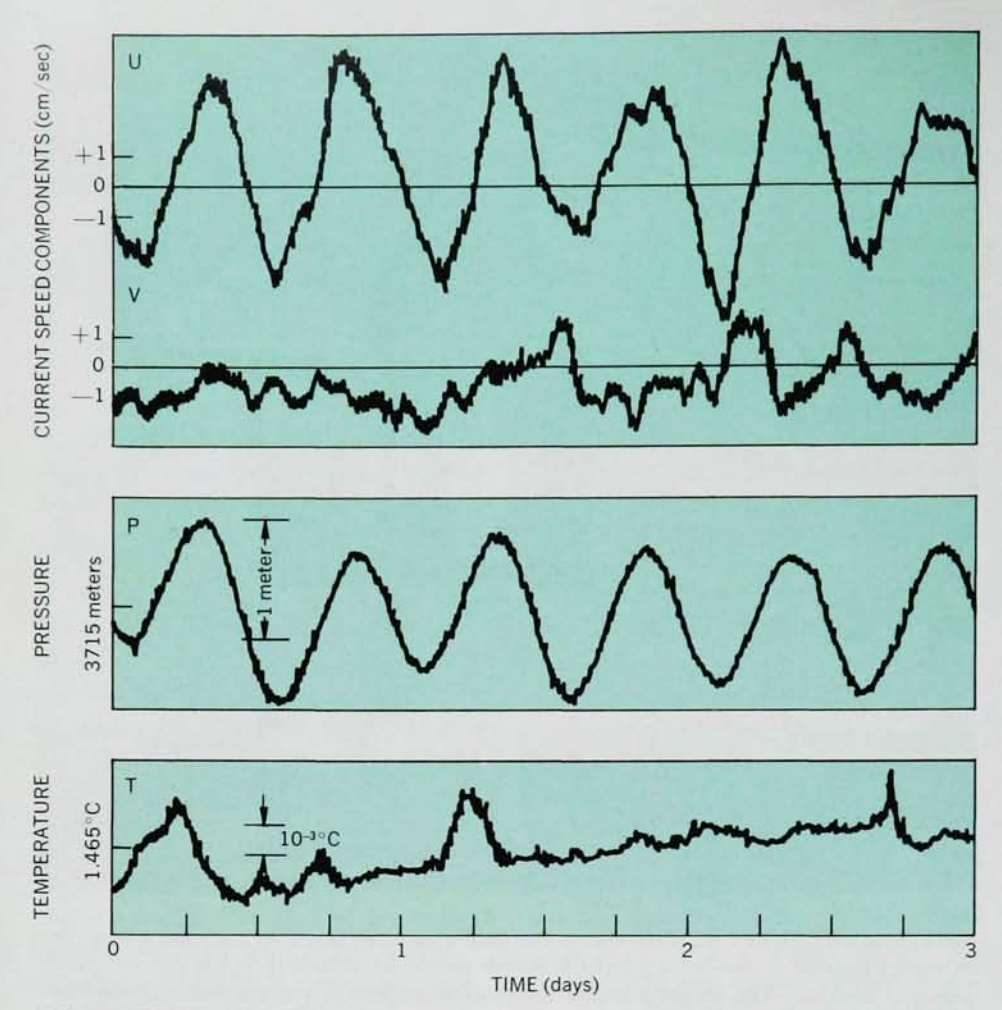
By cycling the pressure between 0 and 8000 psi, we obtain a measurement of the hysteresis. Typically the hysteresis is from 0.01% to 0.2% of the range of the sensor. One assumes that the percentage hysteresis is the same when the pressure is cycled over 1/5500 of this range by the tide signal.

Voltage sensitivity of the sensor is determined at a temperature and pressure approximately equal to that of the sea floor. A value of about 0.13 meters of water pressure per volt is



INSTRUMENT-SUPPORT FRAME as it would appear in place on the ocean floor; the only part missing is the battery-ballast, which would be attached to the release mechanism at bottom. The close-up below shows arrangement of current-meter thermistors, which give speed and direction by measuring temperature differences. —FIG. 3





OCEAN-FLOOR TIDES. Current-component, pressure and temperature data from depth of 3700 meters. Component U is parallel to shore; V is normal. —FIG. 4

typical. With mercury-battery power supplies, the applied voltage decreases only about 0.1 volts resulting in a drift of 1.3 cm, which is small compared to the observed drifts (figure 5). If the battery voltage decreases smoothly, the high-frequency spectral noise introduced through the voltage sensitivity should be small.

Temperature-sensor calibration

We calibrate the crystal temperature sensor using a conventional stirredwater bath with a precision mercuryin-glass or platinum-wire thermometer read to 10^{-4} °C. A polynomial calibration curve is fitted to the data (f vs T) by the least-squares method. We see only a very slight curvature in the calibration curve.

Calibrations at high pressure indicate a negligible pressure effect. Hysteresis and voltage sensitivity are negligible. When calculating the absolute temperature from measurements, full account is taken of the polynomial temperature calibration. When calculating temperature variations after

Table 2. Pressure and Temperature Dependence of Sea-Water Properties

	Property	Symbol	Change for pressure varying from 0 to 500 bars at 2°C (%)	Change when warmed 1°C at 500 bars (%).
Speci	fic heat	$C_{\rm p}$	-6	-0.01
Densi	ty		+2	-0.02
Ther	nal conductivity	K	+2	+0.2
Kiner	natic viscosity	ν	-5	-2
Theri	nal expansion	β	+160	+2
Pranc	Itl number (ν/χ)	Pr	-10	-2
	nal diffusivity	x	+6	+0.2

the capsule has stabilized on the bottom, we use only the slope of the calibration curve at the mean temperature.

Current-meter calibration

The indirectly heated thermistor for water-current measurement that we have just discussed is contained in a copper cylinder 0.635 cm in diameter. Nearby an unheated thermistor in an identical cylinder compensates for temperature changes. The usual formulas for hot wires are applicable. At very low speeds, however, free convection is not negligible because, compared with a hot wire, this sensor is much larger and its aspect ratio (the ratio of length across the flow to thickness along the flow) much smaller.

Characteristics of the sensor are affected by water properties. Table 2 shows pressure and temperature effects on some of them. The thermal-expansion coefficient is extremely dependent on both temperature and pressure, but it only affects sensor response when water is flowing so slowly that free convection is important. Viscosity also changes substantially, especially with temperature, thereby affecting response at all speeds.

Equations for heat transfer from a cylinder to a flowing liquid will be needed when we discuss the effect of water flow on temperature measurements, as well as for this section. The definitions of some symbols are given in table 2. These equations have been found accurate for fine vertical wires in gas flows. For free convection⁵

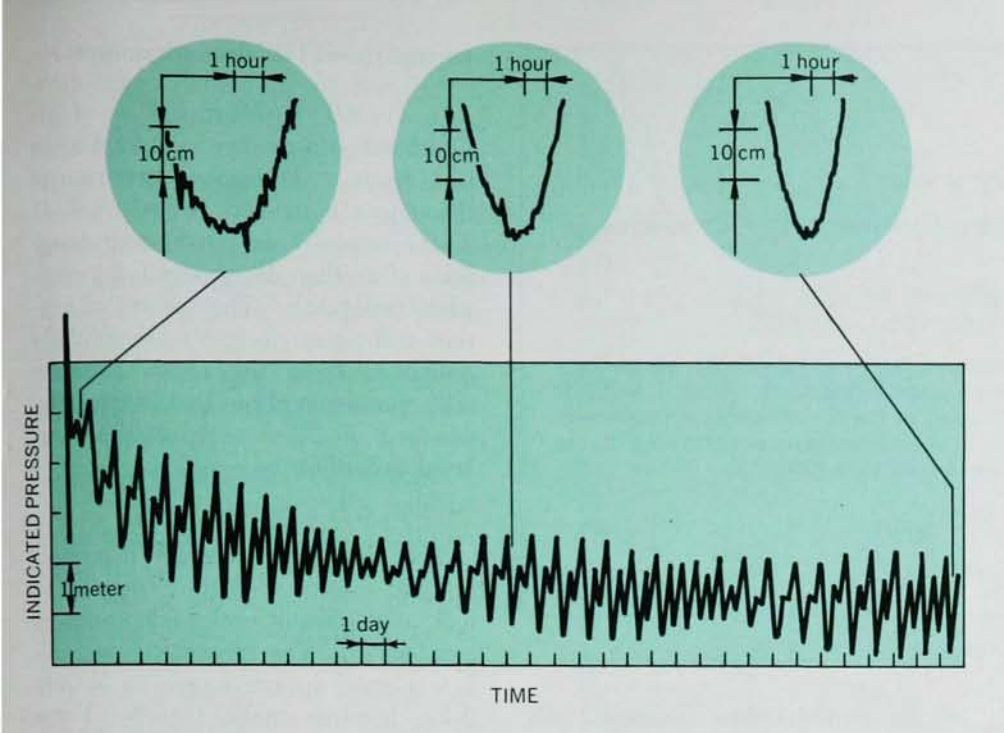
$$Nu = 0.55 (G Pr)^{1/4}$$
 (1)

For forced convection⁶

$$Nu = 0.42 Pr^{0.2} + 0.57 Pr^{1/3} Re^{1/2}$$
 (2)

 $G = \text{Grashof number } g\beta\Delta TD^3/v^2$; $g = \text{acceleration of gravity; } \Delta T = \text{temperature rise in transducer; } D = \text{size of transducer; } Nu = \text{Nusselt number } H/(\pi DK\Delta T)$; $H = \text{heat dissipated in transducer; } Pr = \text{Prandtl number, } v/\chi$; Re = Reynolds number UD/v; U = fluid flow speed.

Equation 1 can be written $\Delta T = CH^{4/5}$. Equation 2 can be expressed as $\Delta T = H/(A + B U^{1/2})$. A, B and C are dependent on fluid properties. These equations give ΔT for no flow and U dependence at high speeds, but there is no equation for the situation in which both free and forced convec-



LONG-TERM DRIFTS. 37-day record from pressure sensor at 3600 meters clearly shows daily tides. Superimposed are a drift towards lower pressure and a diminishing high-frequency noise (apparent in the three enlarged sections at top of figure).—FIG. 5

tion are important. Because of this lack of knowledge and poor precision in measured values of some of the physical properties (thermal expansion for example), a systematic error of perhaps 5–10% in using the calibrations cannot be removed.

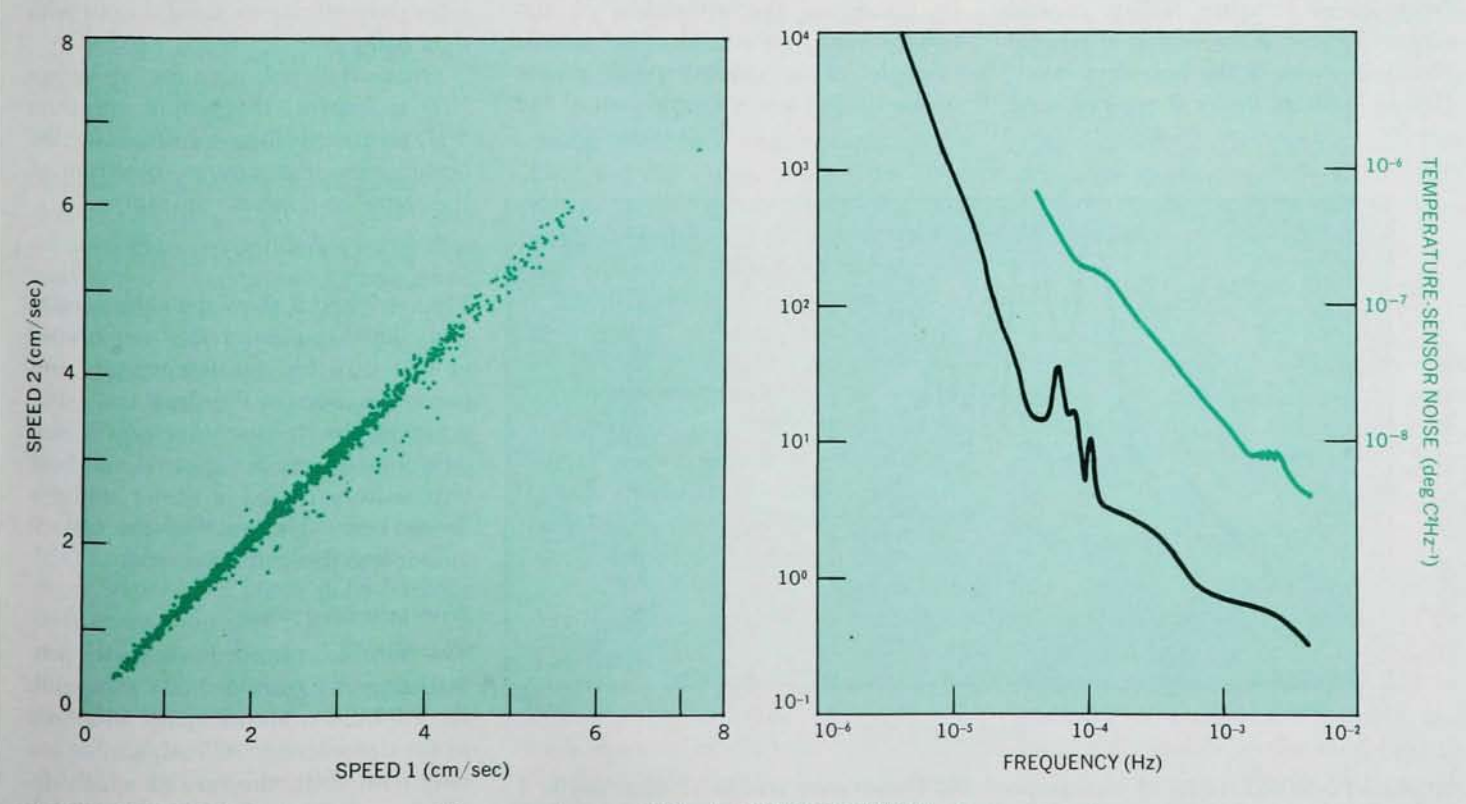
Another possible source of error is the effect of turbulence on heat transfer. Eddies with sizes comparable to that of the transducer have the greatest effect.⁷ Because the response time is far too slow to measure an eddy of this size, we do not know what energy is present at this scale in the ocean. At larger scales, however, the spectrum of turbulent fluctuations shows variation decreasing rapidly as scale decreases.

Fluctuations on a somewhat larger scale also can affect measurements because of bias introduced in averaging a nonlinear response curve. This effect is remarkably small; averaging fluctuations of 20% in amplitude produces only a 1% shift in apparent mean value.⁸

Another problem is flow blockage by transducer and supports. In the calibration channel the water must speed up to compensate for reduced cross section at the transducer location. Flow speed is usually measured elsewhere. For a 6-mm-diameter transducer in a 45-cm-wide channel the effect is just a little over 1%. In the ocean the current will sometimes be flowing over the mounts, which subtend angles of less than 10 deg at the sensor elements, before reaching these elements.

The data (linearly related to ΔT) are recorded digitally and fed to a computer where the nonlinear conversion to U values is simply performed. The nonlinearity of the current sensors is actually an advantage in one important respect. At flow speeds typically found in the deep sea (greater than 0.3 cm/sec) the sensitivity of the sensor increases with decreasing speed. Consequently, at low speeds (about 1 cm/sec) where mechanical devices usually fail, this sensor performs excellently.

Because of the nonlinear characteristics of the current sensors, noise introduced by electronics and least-count considerations depends on water velocity. The least-count speed varies from



REGRESSION PLOT of two sensors 15 cm apart.

-FIG. 6 NOISE SPECTRA of current and temperature sensors. -FIG. 7

UNSCRAMBLING SIGNAL AND NOISE

Let

$$X_{i}(t) = U(t) + n_{i}(t)$$
 $i = 1,2$

represent the output of two sensors. The spectral matrix of these measured outputs is

$$\begin{pmatrix} S_{11}(f) & C_{12}(f) \\ Q_{12}(f) & S_{22}(f) \end{pmatrix} = \begin{pmatrix} X_1(f)X_1^*(f) & \text{Re}[X_1(f)X_2^*(f)] \\ \text{Im}[X_1(f)X_2^*(f)] & X_2(f)X_2^*(f) \end{pmatrix}$$

where X_j represents the Fourier transform of the output X_j of gauge j. Q_{12} vanishes if the gauges have the same response functions. Then if, first, the incoherent parts of the U signals in the outputs of the two sensors are small compared to the noise and, second, the noise in one sensor is incoherent with that in the other, then the noise powers of the two sensors are given by

$$N_{jj}(f) = S_{jj}(f) - S_{UU}(f)$$
 $j = 1, 2$
 $S_{UU}(f) = C_{12}(f)$

0.025 cm/sec at 10 cm/sec to 0.001 cm/sec at 0.5 cm/sec.

On-site recalibrations

Measurement of the vertical current profile requires very good relative accuracy, so recalibrating while on bottom is necessary. For this purpose six current-speed sensors are mounted along a mast held above the bottom by a magnesium link. Failure of the magnesium link caused by electrolysis in the sea water allows the mast to fall after about 25 hours.

Before the mast falls all sensors see approximately the same speed of flow. (A small correction for the elevation of each sensor is made from boundary-layer theory.) After falling, several sensors lie within the region of rapidly changing speed in the boundary layer. Graphs such as figure 6 are prepared

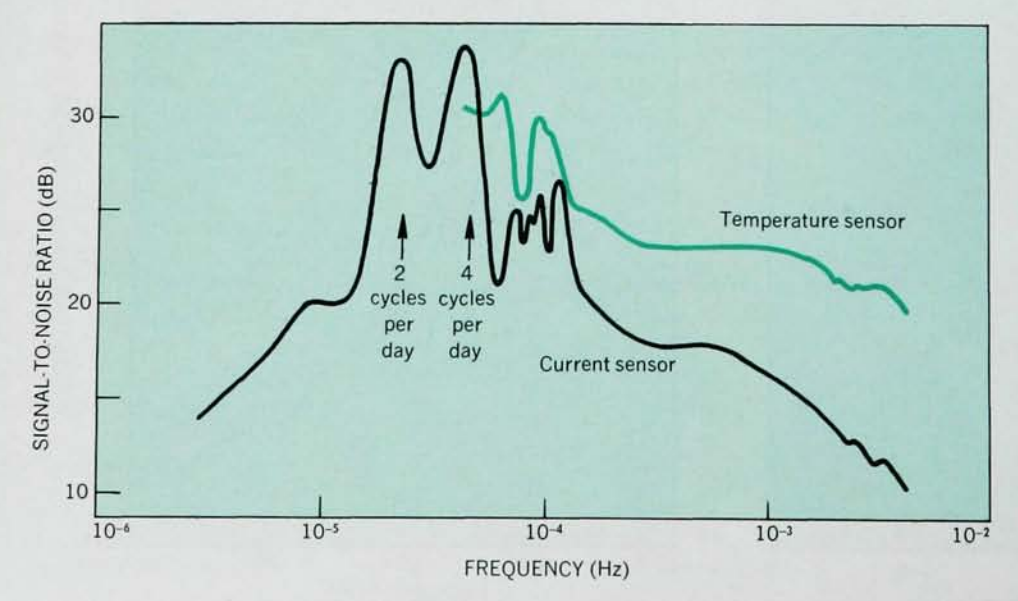
for the period before the mast falls, and these are used as relative calibrations for the data recorded after the mast drops.

In this particular case little correction to the original calibration is required: The points lie close to the 45-deg line. The scatter from the 45-deg line is because of small eddies and occasional shadowing of one transducer by the other.

Similar on-site relative calibrations of temperature sensors are made to permit precise measurements of the vertical temperature gradient just above the sea floor.

Stationary noise

In discussing the estimation of stationary noise, we consider the specific example of a current-speed sensor whose output x is a simple sum of the



SIGNAL-TO-NOISE ratios of current-speed and temperature sensors at 4-km depth, 1 meter above bottom. They are based on the noise spectra shown in figure 7.—FIG. 8

current speed U and sensor noise n

$$x(t) = U(t) + n(t)$$

(Both x and n are here assumed to be in U units.) The power spectrum of the output is defined as $S(f) \equiv X(f)$ $X^*(f)$ where X is the Fourier transform of x (the asterisk signifying complex-conjugate). The spectra of current and noise (S_{UU}, N) are similarly defined. From the above equation and the assumption that n is independent of U, these spectra are related according to

$$S(f) = S_{UU}(f) + N(f)$$

The ideal procedure for determining the noisiness of the sensor is to look at its output under conditions of constant U. The measured spectrum S is a good approximation to N only if S_{UU} is much smaller than N. For a quiet sensor, an environment satisfying S_{UU} much smaller than N in the frequency band of interest may be impractical. Even in an environment for which S_{UU} is greater than N, however, the noise power N may be estimated if a second sensor is used. The equations that govern the situation are worked out in the box on this page.

We must satisfy the two conditions specified in the box as follow: The sensors must be close enough together, and there must be no source of noise common to both sensors, such as a common unregulated power supply. By using redundant sensors in this way you can even make on-site transducer noise determinations simultaneous with data collection.

Once the sensor noise spectrum N(f) is known, the output spectrum S(f) measured "on location" in the ocean gives the desired spectrum of the signal-to-noise power ratio

$$[S(f) - N(f)]/N(f).$$

Figures 7 and 8 show the noise spectra and signal-to-noise ratios determined in this way for our temperature and current sensors in the deep sea. The noise of the temperature sensor was determined from the spectral matrix of two sensors buried a meter under a flower bed. The noise of the current sensor was determined on site.

Nonstationary noise

The Vibrotron noise is distinctly nonstationary. Figure 5 shows a 1-month record from a rather noisy Vibrotron in the deep ocean. Clearly visible is a long-term drift, the rate of which decreases with time, and a high-frequency noise, which also decreases with time. The form of the drift is fairly well represented as $a(t-t_0)^{1/3}$ where a is a constant and t_0 is the time at which the sensor was dropped to the ocean bottom. Although mechanical creep has this $t^{1/3}$ form, pressure-induced creep probably is not the cause of the drift. There are several pieces of evidence:

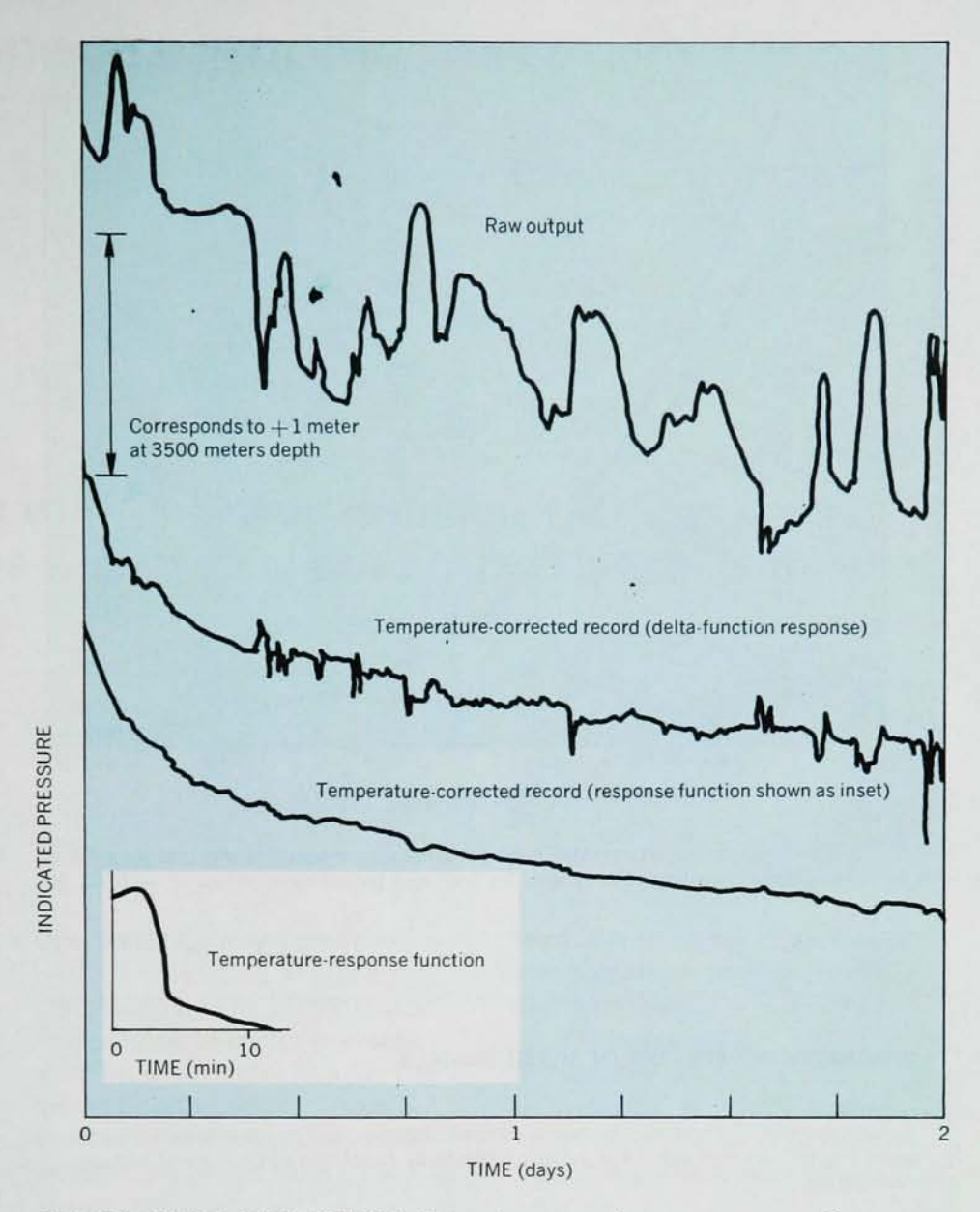
- The drift may be towards apparently higher or lower pressures (although for a given sensor it is always in the same direction).
- The drift is too great for ordinary stress-induced mechanical creep to account for it.
- Even a sensor with its pressure port capped shows this drift when installed on the ocean bottom (figure 9).
- That a similar drift can be produced in the laboratory simply by rapidly cooling the sensor suggests that temperature rather than pressure change is the cause of the problem. The sensor is made from dissimilar materials, and at the junctions of these materials temperature changes can produce large stresses that are then slowly released by some sort of plastic deformation.

The record from a quartz-crystal temperature sensor occasionally contains sudden jumps corresponding to temperature steps as large as 10^{-3} °C. These jumps seem to occur only in a few particular sensors. They are probably caused by sudden spontaneous changes in the quartz-crystal structure. (The manufacturer is replacing crystals for us on the assumption that this explanation is true.)

Secondary sensitivities

A sensor may have a troublesome secondary sensitivity, that is, sensitivity to an environmental parameter other than that which it is supposed to measure. For example, an oceanographic pressure sensor may be temperature sensitive and a temperature sensor may be pressure sensitive. The equations with which we treat such secondary sensitivities are shown in the box on page 42.

The temperature-response function b(t) represents the response of a linear sensor to a Dirac delta-function temperature input, $T(t) = \delta$ (t). It may be measured in the laboratory by subjecting the sensor to a temperature step function and differentiating the output signal. In slow flows such as the deep sea, however, the boundary layer around the sensor may signifi-



TEMPERATURE CORRECTION of data from capped pressure sensor. One can assume a delta function or use a response function determined on site.

—FIG. 9

cantly affect heat transfer between the fluid and the sensor. Hence the effective b(t) depends on the flow speed. In the deep sea an on-site method of determination is clearly desirable.

To determine the pressure sensor's temperature response function $b_1(t)$ for sea-bottom conditions, the sensor was capped, effectively making α_1 equal to 0, and its output was recorded together with the output of a nearby temperature sensor. The temperature sensor's response is rapid compared with the sampling interval used (2 minutes), and its pressure sensitivity is negligible. So to a good approximation, $\alpha_2 = 0$, $b_2(t) =$ $\beta_2 \delta(t)$; β_2 is readily measured in the laboratory calibration. The sensors were installed at the relatively shallow depth of 400 meters. At this depth the temperature fluctuations are much

stronger than in the deep sea so that sensor noise can be neglected. $b_1(t)$ is given by the inverse Fourier transform of $B_1(t)$ obtained from

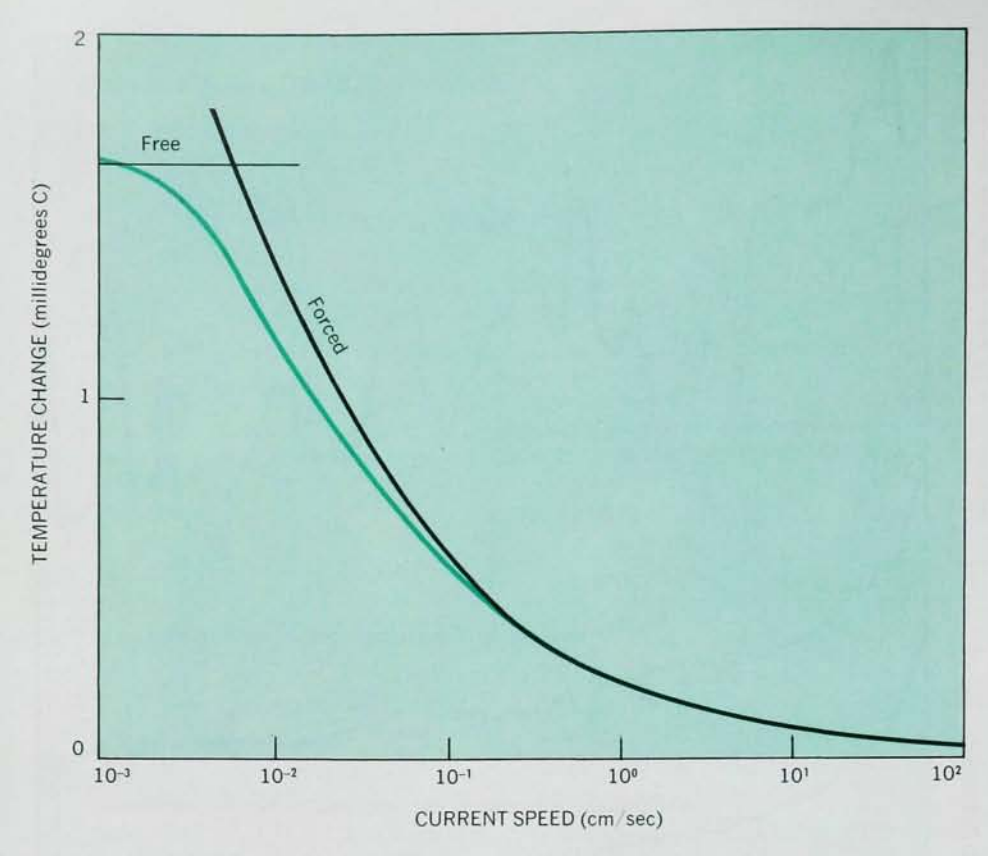
$$S_{22}(f) = \beta_2^2 S_{TT}(f)$$

 $S_{12}(f) = B_1(f) \beta_2 S_{TT}(f)$

by eliminating $S_{TT}(f)$. To remove the temperature component from the pressure-sensor output, the resulting b_1 convolved with T is subtracted from the data (figure 9).

Anemometer effect

Any temperature-sensitive device placed in a fluid will be sensitive to the speed of flow. Even if no heat is dissipated in the transducer, it will be warmed by compressive heating and viscous dissipation in the fluid near its surface. The magnitude of these effects in sea water is calculated as fol-



SELF-HEATING of the quartz crystal used in temperature-sensitive devices as a function of current speed, showing the ranges for free and forced convection. —FIG. 10

UNSCRAMBLING SPECTRA OF MIXED SIGNALS

If, for example, both of two sensors respond linearly both to pressure and temperature, we can represent the sensor outputs as functions of time t and history τ as follows

$$x_1(t) = \alpha_1 P(t) + \int_{-\infty}^{\infty} b_1(\tau) T(t+\tau) d\tau + n_1(t) + \gamma_1$$

$$x_2(t) = \alpha_2 P(t) + \int_{-\infty}^{\infty} b_2(\tau) T(t+\tau) d\tau + n_2(t) + \gamma_2$$

We assume pressure responses are immediate. As temperature responses are dependent only on past temperatures, b_1 and b_2 are zero for $\tau>0$. If the pressure sensitivities α_1 , α_2 and the temperature response functions b_1 , b_2 are different for the two gauges, and if the noise spectra $N_{11}(f)$, $N_{22}(f)$ are known, then from the data spectral matrix

$$\begin{pmatrix} S_{11}(f) & C_{12}(f) \\ Q_{12}(f) & S_{22}(f) \end{pmatrix}$$

the geophysical P, T spectral matrix

$$\begin{pmatrix} S_{PP}(f) & C_{PT}(f) \\ Q_{PT}(f) & S_{TT}(f) \end{pmatrix}$$

can be calculated in principle. For, by Fourier transforming the auto- and cross-covariance functions of x_1 and x_2 , one gets the following four equations

$$\begin{aligned} \mathbf{S}_{jj} &= \alpha j^2 \mathbf{S}_{PP} + 2 \alpha_j \mathrm{Re}[\mathbf{B}_j ^* \mathbf{S}_{PT}] + |\mathbf{B}_j|^2 \mathbf{S}_{TT} + \mathbf{N}_{jj} \\ & \text{(two equations, } j = 1 \text{ and } 2) \end{aligned}$$

$$S_{12} = \alpha_1 \alpha_2 S_{PP} + \alpha_1 B_2 * S_{PT} + \alpha_2 B_1 S_{PT} * + B_1 B_2 * S_{TT}$$

(two equations, real and imaginary parts)

If the α_j , b_j (or B_j) and N_{jj} are known, these equations can be solved for the four unknowns S_{PP} , S_{TT} , C_{PT} , Q_{PT} , at each frequency f. (B_j is the Fourier transform of b_{jj} , $S_{12} = C_{12} + iQ_{12}$ and $S_{PT} = C_{PT} + iQ_{PT}$.)

lows (U is speed in cm/sec; ΔT is temperature rise in degrees centigrade)

 ΔT (compressive heating) = $\rho U^2/2$ × compressibility/thermal expansion \approx $2 \times 10^{-6} \times U^2$

$$\Delta T$$
 (viscous heating) = $5U^2 \rho/8C_p \approx 2 \times 10^{-7} U^2$

These effects amount to only tens of microdegrees in ocean-bottom conditions, but they illustrate the problems one encounters when pushing techniques to the limit.

In any real transducer, heat dissipated electrically will produce much larger temperature rises. The temperature-sensitive crystal oscillator we have used dissipates only about 100 microwatts in the crystal itself. At first the crystal was in the same case with the electronics, which dissipated much more heat. Later models have the crystal isolated to decrease this effect. The pressure gauge was also modified by thermally isolating the amplifier (the chief dissipating component) from the sensitive element. Equations 1 and 2 are relevant here. They show that the temperature rise in a transducer of approximately 2-cm size that dissipates 100 microwatts will be as given in figure 10. Variations in warming shown are not much less than the real temperature variation in the ocean-bottom water. The addition of a heat sink increases the effective area through which this heat must be transferred and should reduce the effect by a factor of ten. Because of the difficulty of providing an environment with small enough temperature fluctuations, we cannot measure these effects in the laboratory.

References

- W. H. Munk, F. E. Snodgrass, M. J. Tucker, Bull. Scripps Inst. Oceanog. 4, 283 (1959); F. E. Snodgrass, Science 146, 198 (1964); W. H. K. Lee, C. S. Cox, J. Geophys. Res. 71, 2101 (1966).
- F. E. Snodgrass, Science 162, 78 (1968).
- D. R. Caldwell, Rev. Sci. Instr. 39, 1865 (1968).
- 4. M. H. Wimbush, W. H. Munk, "The Benthic Boundary Layer," *The Sea*, Vol 4, Interscience, New York (in press).
- H. Schlichting, Boundary-layer Theory, 6th edition, McGraw-Hill, New York (1968) p. 303.
- 6. J. O. Hinze, *Turbulence*, McGraw-Hill, New York (1959) p. 76.

- 7. Ref. 6, p. 559.
- 8. Ref. 6, p. 97.